Evaluation and Comparison of Daily GPM/TRMM Precipitation Products over the Tianshan Mountains in China

Yin Zhang [1,2,3] **, Gulimire Hanati** [4] **, Sulitan Danierhan** [1,2,*] **, Qianqian Liu** [1,2,3] **and Zhiyuan Xu** [5]

1   State Key Laboratory of Desert and Oasis Ecology, Xinjiang Institute of Ecology and Geography, Chinese Academy of Sciences, Urumqi 830011, China; zhangyin17@mails.ucas.ac.cn (Y.Z.); liuqianqian215@mails.ucas.ac.cn (Q.L.)
2   Akesu National Station of Observation and Research for Oasis Agro-Ecosystem, Akesu 843017, China
3   University of Chinese Academy of Sciences, Beijing 100049, China
4   Xinjiang Institute of Water Resources and Hydropower Research, Urumqi 830049, China; skyglml@163.com
5   College of Water Conservancy and Civil Engineering, Xinjiang Agricultural University, Urumqi 830052, China; Xu18160666361@163.com
*   Correspondence: sulitan@ms.xjb.ac.cn

Abstract: Based on the complex topography and climate conditions over the Tianshan Mountains (TSM) in Xinjiang, China, the new precipitation product, the Global Precipitation Measurement (GPM) (IMERG), and its predecessor, the Tropical Rainfall Measuring Mission (TRMM) 3B42 (TMPA), were evaluated and compared. The evaluation was based on daily-scale data from April 2014 to March 2015 and analyses at annual, seasonal and daily scales were performed. The results indicated that, overall, the annual precipitation in the Tianshan area tends to be greater in the north than in the south and greater in the west than in the east. Compared with the ground reference dataset, GPM and TRMM datasets represent the spatial variation of annual and seasonal precipitation over the TSM well; however, both measurements underestimate the annual precipitation. Seasonal analysis found that the spatial variability of seasonal precipitation has been underestimated. For the daily assessment, the coefficient of variation (CV), correlation coefficient (R) and relative bias (RB) were calculated. It was found that the GPM and TRMM data underestimated the larger CV. The TRMM data performed better on the daily variability of precipitation in the TSM. The R and RB data indicate that the performance of GPM is generally better than that of TRMM. The R value of GPM is generally greater than that of TRMM, and the RB value is closer to 0, indicating that it is closer to the measured value. As for the ability to detect precipitation events, the GPM products have significantly improved the probability of detection (POD) (POD values are all above 0.8, the highest is 0.979, increased by nearly 17%), and the critical success index (CSI) (increased by nearly 9% in the TSM) is also better than TRMM, although it is only slightly weaker than TRMM in terms of the false alarm ratio (FAR) and frequency bias index (FBI). Overall, GPM underestimates the low rainfall rate by 6.4% and high rainfall rate by 22.8% and overestimates middle rain rates by 29.1%. However, GPM is better than TRMM in capturing all types of rainfall events. Based on these results, GPM-IMERG presents significant improvement over its predecessor TRMM 3B42. Considering the performance of GPM in different subregions, a lot of work still needs to be done to improve the performance of the satellite before being used for research.

Keywords: GPM; TRMM; Tianshan Mountains; spatial distribution of precipitation; precipitation estimation

1. Introduction

Precipitation is a fundamental component of the global water cycle. It provides important information for climate research, water resource management and many other applications, and plays an important role in the interaction between the hydrosphere, atmosphere, and biosphere [1]. Due to the great spatial and temporal variability of precipitation, accurate precipitation measurements remain challenging, especially in regions with complex topography [2,3]. Three methods have been commonly used to measure precipitation: rain gauges, weather radars and satellite sensor. A rain gauge measures precipitation directly and is considered to be the most accurate method of determining rainfall; however, as the ground stations are sparsely distributed, rain gauges have accuracy limitations because they measure rainfall at a single point, which is insufficient to accurately describe the spatial variability of precipitation [4].

The emergence of multisatellite inversion technology provides a new method for rapidly capturing precipitation information. Satellite data are the most effective means of precipitation observation on a global scale [5]. Because precipitation observation satellites generally have the characteristics of real-time, average spatial distribution, wide coverage, and high temporal and spatial resolution, they have gradually been applied to various meteorological and hydrological research [6,7]. Among them, the Tropical Rainfall Measuring Mission (TRMM) has been widely used due to its relatively high accuracy [8–13]. As the successor of TRMM, the Global Precipitation Measurement (GPM) Mission initiated by NASA and JAXA was launched in April 2014. It can explore the characteristics of global precipitation in a more detailed and advanced way [14,15].

In recent years, numerous studies have been conducted worldwide to evaluate the performance of GPM. For example, Jiang et al. [5] used the humid Mishui basin in the mid-latitude of southern China as the research area to evaluate the products of GPM-IMERG's early, late and final run and reported that the IMERG datasets are superior to TMPA. Wang et al. [16] compared and assessed different versions of GPM-IMERG, providing global and regional evaluation results for GPM algorithm developers and insights for users of the global GPM product. Mahmoud et al. [17] verified the performance of GPM over the United Arab Emirates (UAE) based on observation data from surface rain gauges. They believed that the final-run-product of GPM-IMERG not only better reflected the rainfall variability and patterns in UAE but also had potential uses for complementing or replacing the ground rainfall measurements. Wu et al. [18] quantitatively evaluated the accuracy of GPM and TMPA over the Yangtze River basin, indicating that both IMERGV5 and 3B42V7 overestimated precipitation in low-elevation areas. A few studies exist regarding the product's ability to detect and estimate precipitation and extreme precipitation. Prakash et al. [3] compared 17-year TMPA data with GPM-IMERG data to study these products' abilities to detect and estimate heavy rainfall across India. It was concluded that the quality of GPM research product for detecting the frequency of rainstorm events across India significantly improved TMPA during the southwest monsoon season. Fang et al. [19] reported that the GPM and TMPA capture the spatial patterns of extreme precipitation in China. GPM is generally better than TMPA. Zhang et al. [4] reported that satellite products (IMERG/GSMAP) generally capture the temporal and spatial patterns of rainstorms, but both underestimate the accumulated precipitation of storms.

Satellite precipitation products have greatly facilitated the estimation of precipitation at global and regional scales, especially in areas with few surface rain gauges and poor performance of other traditional methods [20]. Recently, several scholars have studied the results of satellite precipitation products from different regions around the world [1,17,21]. The results of these studies have shown that IMERG products are closely related to regional topography and climatic conditions when describing precipitation. For example, Wang et al. [1] showed that topography impacts the performance of IMERG/TMPA data, overestimating precipitation in low-elevation areas and underestimating it in high-altitude areas. Caracciolo et al. [21] found that the accuracy of GPM is related to topography. Mahmoud et al. [17] reported that the eastern and northeastern parts of the UAE have complicated terrain; thus, satellite products perform poorly in these areas.

In this context, it is critical to verify the satellite datasets over different terrain and climatic regions. Because GPM products have only been launched in recent years, the terrain of the Tianshan mountainous (TSM) is complex, and there are few comprehensive assessments based on daily-scale data at the subregion level, the application of GPM products in the TSM area has remained limited. Therefore, this study evaluates and compares the estimation accuracy of the two satellite precipitation datasets GPM-IMERG and TRMM 3B42 in the TSM. This assessment uses the China Gauge-based Daily Precipitation Analysis (CGDPA) as the ground reference dataset, which is a set of daily precipitation grid products in China launched by the National Meteorological Information Center (NMIC) of China Meteorological Administration (CMA). It is a comprehensive observational daily precipitation report database. The study period was from April 2014 to March 2015.

2. Study Area

The Tianshan Mountains (TSM) are located in Central Asia and northwest China. In China, the TSM are located from 34.34° to 55.43° N and from 75° to 96.37° E [22]. The mountain range extends approximately 1700 km from east to west and 400 km from north to south [23,24] and is an important demarcation line between southern Xinjiang and northern Xinjiang in China [25], which form two different natural landscapes. The TSM are far from the ocean, with little precipitation and extremely uneven distribution [26]. The average annual precipitation is 180 mm in the whole region, but the average annual precipitation of the northern slope is more than 200 mm, and that of the southern slope is about 150 mm [27]. The daily temperature variations is large, which is a typical continental climate [28–30]. The height and orientation of the TSM have an important influence on weather patterns, precipitation distribution and precipitation forms [31]. The topography of the TSM is complex, and the precipitation is closely related to the topography. The topography plays a vital role in forming a distinct local climates. The precipitation in the north of the TSM is larger than that in the south, the mountain area is larger than the plain, and the largest precipitation occurs in the Yili Valley. In terms of temperature distribution, the northern slope of the TSM is colder than the southern slope, and the western slope is colder than the eastern slope.

Based on the geographical location and climatic conditions of the study area, the Tianshan Mountain is divided into three parts: the west, with the highest peak of 7435 m, the east (TS4) with the maximum peak of 5445 m, and the middle section (TS3) (Figure 1) [31]. The western Tianshan Mountains are further subdivided into northwest Tianshan (TS1) (including Boertala Valley and Yili Valley) and southwest Tianshan (TS2) according to the seasonal and annual precipitation distribution (Figure 2). The four subregions are consistent in precipitation change and seasonal circulation pattern.
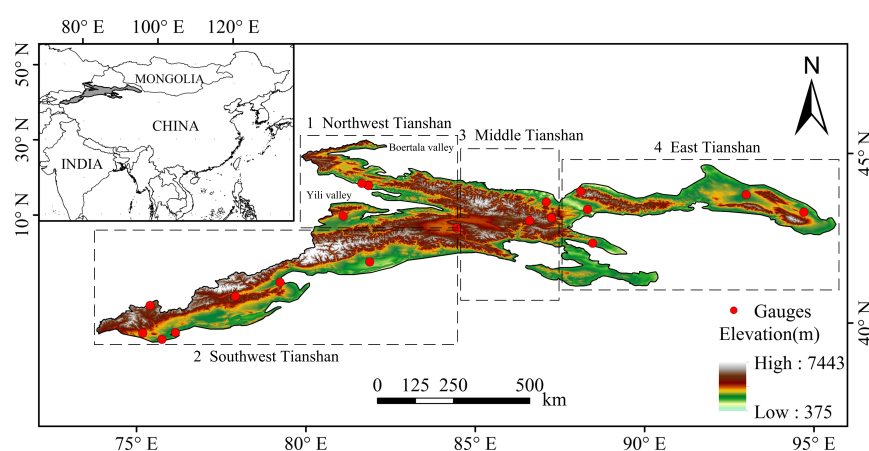

Figure 1. Location and topographic features of Tianshan Mountains and distribution of rain gauges. The black dashed line indicates the range of the four subregions: 1 Northwest Tianshan (TS1), 2 southwest Tianshan (TS2), 3 middle Tianshan (TS3), and 4 east Tianshan (TS4) (Base on map sources: GS (2020) 3183).
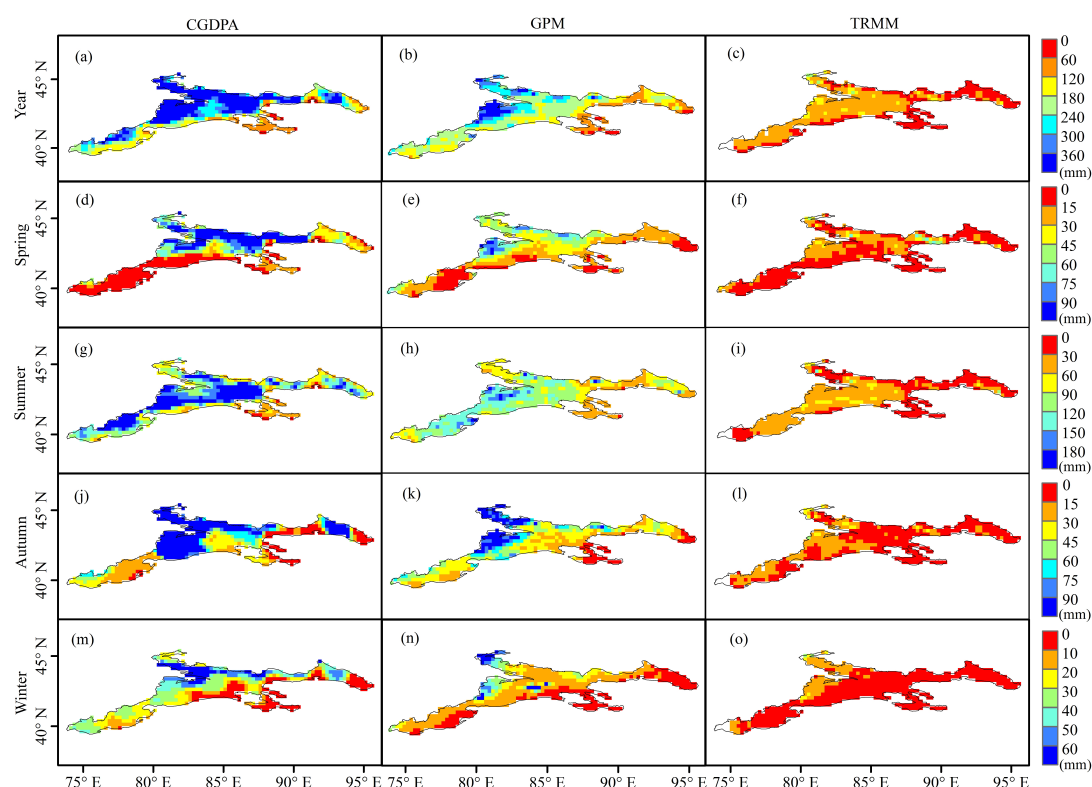
Figure 2. Spatial distribution of annual and seasonal total precipitation (mm) by the China Gauge-based Daily Precipitation Analysis (CGDPA) (**a**,**d**,**g**,**j**,**m**), the Global Precipitation Measurement (GPM) (**b**,**e**,**h**,**k**,**n**), and the Tropical Rainfall Measuring Mission (TRMM) (**c**,**f**,**i**,**l**,**o**) in the Tianshan Mountains (TSM) of China from 1 April 2014 to 31 March 2015. Year (**a**–**c**), spring (**d**–**f**), summer (**g**–**i**), autumn (**j**–**l**), winter (**m**–**o**).

3. Materials and Methods

3.1. Rainfall Datasets

3.1.1. GPM Data

The Global Precipitation Measurement (GPM) mission is a newly launched international satellite network providing global rainfall and snow observations. Compared with previous satellite precipitation products, GPM has higher accuracy and spatiotemporal resolution. On the basis of TRMM's success, it deployed a "core" satellite with an advanced radar/radiometer system to measure spatial precipitation and serves as a reference standard for unified research and operational satellite constellation precipitation measurements to improve our understanding of the Earth's water and energy cycle and our ability to predict extreme events for the benefit of society.

The GPM satellite carries two main sensors: the GPM Microwave Imager (GMI) and a Dual-Frequency Precipitation Radar (DPR) [32]. The input precipitation estimates are calculated by various passive microwave and infrared satellite sensors. According to the demand, it has three different modes: an early, late and final run. Among them, the final-run dataset introduces monthly gauge analysis for deviation correction, which is generally considered to be more accurate than early and late run, and is widely used in hydrological and climate research [19].

IMERG data are one type of GPM data. The latest version of the IMERG final-run product V06 is used, which was launched in April 2014. This product has a spatial resolution of $0.1° \times 0.1°$ and a coverage of 60° N–60° N. (Source: https://gpm.nasa.gov/data/directory).

3.1.2. TRMM Data

The Tropical Rainfall Measuring Mission (TRMM), as the predecessor of GPM, is a joint mission launched by NASA and JAXA in 1997 to study rainfall in tropical regions. It is a research satellite that aims to help us understand the precipitation distribution and changes in tropical regions. TRMM has accumulated a large amount of precipitation data with high temporal and spatial resolution, and is widely used in various precipitation studies [33–35].

TMPA data are one type of TRMM data; they have a spatial resolution of 0.25° × 0.25° and a coverage range of 50° N–50° N. The daily dataset selected in this study was accumulated from the research-quality 3-hourly TRMM (TMPA) rainfall estimate. (Source: https://disc.gsfc.nasa.gov/datasets).

3.1.3. CGDPA Data

The China Gauge-based Daily Precipitation Analysis (CGDPA) is produced and routinely calibrated by the National Meteorological Information Center (NMIC) of China Meteorological Administration (CMA). The CGDPA dataset has a daily spatiotemporal resolution of 0.25° and is used as a reference for evaluating the GPM products. This dataset includes daily precipitation from 2419 stations (including the National Climate Observatory, National Meteorological Observation Station I, Second-level station), and the optimal interpolation method based on "climate background field" is applied to generate a grid product of daily precipitation in China in real time [36].

Considering that the GPM satellite datasets started in April 2014 and the TRMM data were stopped in April 2015, we chose the overlap period of the two satellite data from April 2014 to March 2015 as the study period. On the daily scale, a more detailed and comprehensive assessment was made in different subregions.

3.2. Methodology

Since the resolution of GPM datasets are 0.1° × 0.1°, and the resolution of TRMM and the CGDPA datasets are 0.25° × 0.25° resolution, for convenience of analysis, we used the bilinear interpolation method to resample the GPM dataset to 0.25° × 0.25° with the same spatial resolution [24], as shown in Figure 2.

To evaluate and compare the remote sensing satellite dataset against the ground reference dataset, the following indicators were computed: the coefficient of variation (CV), correlation coefficient (R), relative bias (RB) and root mean square error (RMSE). The calculation formulas are shown in Table 2. The CV is used to measure the change of daily precipitation with respect to its daily mean. R evaluates the degree of linear correlation between two datasets. RB describes the systematic deviation of satellite dataset: positive values indicate that the rainfall is overestimated, while negative values indicate that the rainfall is underestimated. RMSE measures the average absolute error of the GPM/TRMM. The smaller the RMSE value, the closer the precipitation measured by the satellite is to the measured value [24].

Accurately describing the frequency of precipitation at various intensities is essential when studying hydrological processes, making climate predictions and assessing land–atmosphere interactions. In this study, the precipitation intensity evaluation was used the probability density function (PDF) method [37]. PDF is calculated as the ratio of the number of precipitation to the total number of precipitation between two continuous thresholds. The calculation formula is shown in Table 2. In addition, in order to better describe the seasonal variation of precipitation, a Taylor diagram is drawn, which reflects the ratio of R, RMSE and SD between estimated and observed precipitation.

In addition to basic statistics, to further evaluate the precipitation detection ability, based on Table 1, the probability of detection (POD), false alarm ratio (FAR), frequency bias index (FBI) and critical success index (CSI) are computed [24]. When the POD, FBI and CSI are close to 1 and the FAR is close to 0, the estimation is highly accurate. The calculation formulas are shown in Table 2. In this study, the adopted threshold is 0.5 mm, and it is assumed that the daily rainfall is less than 0.5 mm as "no rain".

Table 1. A 2 × 2 contingency table for two types of precipitation estimation.

	Observed ≥ 0.5 mm	Observed < 0.5 mm
Estimated ≥ 0.5 mm	H	F
Estimated < 0.5 mm	M	Z

Note: H is the observed precipitation detected correctly by the satellite, F is the observed precipitation detected incorrectly by the satellite, M is the observed precipitation missed by the satellite, and Z represents a correct estimate of no rain.

Table 2. List of the statistical indicators.

Name (Symbol)	Formula	Optimal Value
Correlation Coefficient (R)	$R = \dfrac{\sum\limits_{i=1}^{n}(x_i-\bar{x})(y_i-\bar{y})}{\sqrt{\sum\limits_{i=1}^{n}(x_i-\bar{x})^2 \cdot \sum\limits_{i=1}^{n}(y_i-\bar{y})^2}}$	1
Relative Bias (RB/%)	$RB = \dfrac{\sum\limits_{i=1}^{n}(x_i-y_i)}{\sum\limits_{i=1}^{n}y_i} \times 100\%$	0
Coefficient of Variation (CV/%)	$CV = \dfrac{\sigma}{\mu} \times 100\%$	\
Root Mean Square Error (RMSE)	$RMSE = \sqrt{\dfrac{\sum_{i=1}^{n}(x_i-x)^2}{n}}$	0
Probability of Detection (POD)	$POD = \dfrac{H}{H+M}$	1
False Alarm Ratio (FAR)	$FAR = \dfrac{F}{H+F}$	0
Frequency Bias Index (FBI)	$FBI = \dfrac{H+F}{H+M}$	1
Critical Success Index (CSI)	$CSI = \dfrac{H}{H+M+F}$	1

Note: n = number of samples, σ = standard deviation of the samples, μ = the sample average, x_i = the estimated precipitation by satellites, y_i = the measured precipitation on the ground.

4. Results

4.1. Annual and Seasonal Assessments

Figure 2 shows the total annual precipitation and total seasonal precipitation in different seasons based on the CGDPA, GPM and TRMM datasets in the TSM of China in 2014 accumulated from daily precipitation data. It can be seen from Figure 2 that there are obvious spatial differences of precipitation in different regions. The three groups of data have similar spatial patterns. According to the observations, the annual precipitation decreased from over 600 mm in the rainy northwest TSM area (TS1) to less than 100 mm in the east, especially in the vicinity of the Yili Valley. Although the Yili Valley is far from the ocean, its open westward (horn-shaped) topography is conducive to receiving humid water vapor from the Atlantic Ocean. Every year, westerly airflow enters the Yili Valley in spring, climbing from low to high. The airflow changes from warm to cold in the Piedmont zone, causing abundant precipitation. The spatial patterns of seasonal precipitation is higher in the northwest and lower in the east, and the precipitation is concentrated in summer. Overall, the annual precipitation in the TSM area shares certain common characteristics: precipitation is greater in the north than in the south and greater in the west than in the east. There is good agreement between the satellite precipitation estimates (GPM/TRMM) and the ground reference dataset (CGDPA) about annual precipitation. The spatial distribution of seasonal precipitation is similar to that of annual precipitation.

The precipitation measured in the TRMM dataset is lower than the CGDPA measured in the ground, while the precipitation in the GPM dataset is significantly higher and closer to the true value. Notably, the spatial distribution of annual precipitation from GPM is subtler than that of TRMM. The geometry and distribution of the high precipitation areas over the northwestern part of the Tianshan Mountains is captured better in the GPM datasets than in the TRMM estimates.

4.2. Daily Assessments

To investigate the variation characteristics of daily precipitation, the CV was calculated for each dataset, as shown in Figure 3. The CV can reflect the change in daily precipitation relative to the daily mean. As Figure 3 shows, in the northwest Tianshan (TS1) and middle Tianshan (TS3) areas, the observed CV is small, while in the southwest Tianshan (TS2) and east Tianshan (TS4) areas, the observed CV is large. Generally, larger (smaller) CV values are observed in areas with lower (higher) daily rainfall.

Figure 3. Spatial distribution of CV values (%) of daily precipitation in Tianshan from 1 April 2014 to 31 March 2015.

The GPM and TRMM datasets significantly underestimated the larger CV over southwest Tianshan and east Tianshan. Overall, the TRMM data are more consistent with the daily variability of precipitation in this area.

In Figures 4 and 5, the spatial distribution of R values and relative deviation (RB) of the GPM/TRMM and ground reference dataset (CGDPA) on a daily scale are compared. Overall, the satellite datasets have a good correlation with the measured precipitation (CGDPA) in the east Tianshan (TS4) area. At the same time, the lower R values are mainly found in the western and northern Tianshan Mountains. The combination of Figures 1 and 4 shows that the R value is lower in high-elevation areas and higher in low-elevation areas. Figure 5 shows that the positive and negative deviations of the GPM data are relatively balanced, while TMPA appears as a negative deviation on most gauges. The GPM and TRMM datasets tend to underestimate the daily precipitation in the TSM. In comparison, the precipitation estimates of the GPM dataset are closer to the measured dataset, indicating that the GPM satellite is more accurate in capturing precipitation information. Overall, except for RB, other statistical indicators from GPM and TRMM have similar spatial trend changes. Additionally, it is not difficult to see that these GPM indices are better than those of TRMM and that satellite precipitation datasets performs poorly at high altitudes.
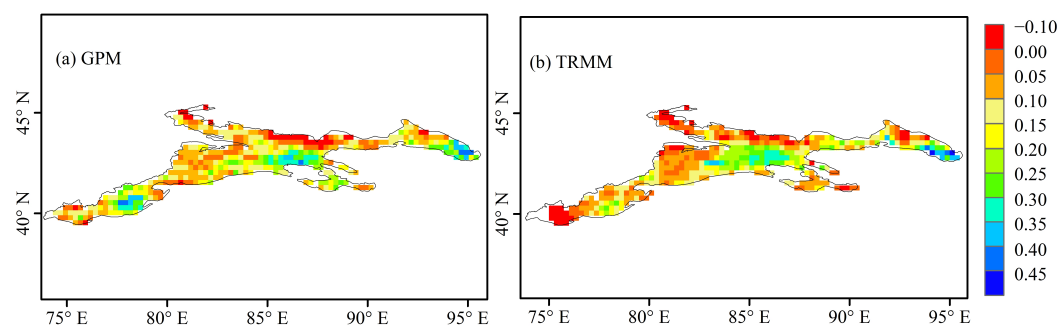

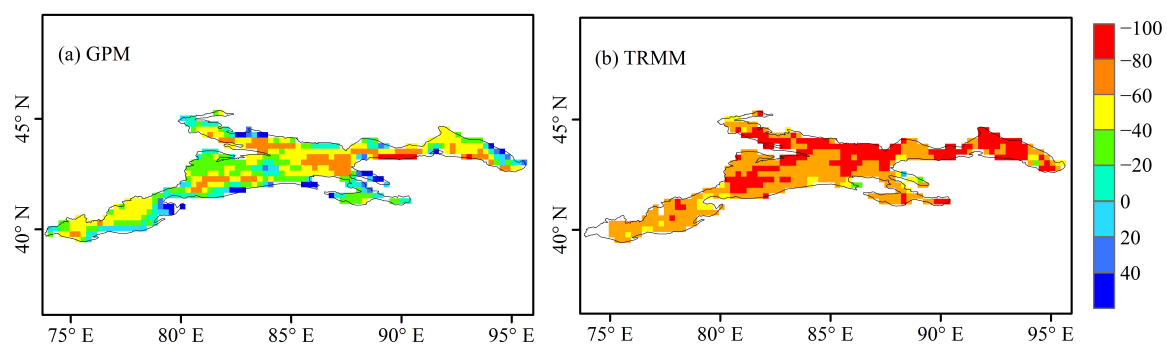**Figure 4.** Correlation between GPM, TRMM and CGDPA from 1 April 2014 to 31 March 2015.

Figure 5. Relative deviation percentage of GPM, TRMM and CGDPA from 1 April 2014 to 31 March 2015.

4.3. Annual Variability and the Seasonal Cycle

Annual variability is significant in areas with low precipitation. In order to further test the ability of satellites to describe the temporal variability of precipitation in the TSM, we analyzed the annual precipitation changes in different subregions based on the GPM/TRMM datasets, as shown in Figure 6. The seasonal distribution of precipitation in the TSM is uneven. The precipitation is mainly concentrated in summer and reaches its minimum in winter, especially in TS3 and TS4. Compared with the ground observations, the satellite datasets portray the annual variability of precipitation well, especially in TS2 and TS3, achieving high correlations (above 0.9). However, both of the satellite products underestimate the annual precipitation. Overall, GPM and TRMM have similar statistical behaviors, but GPM has a lower RMSE in the four subregions and performs better.
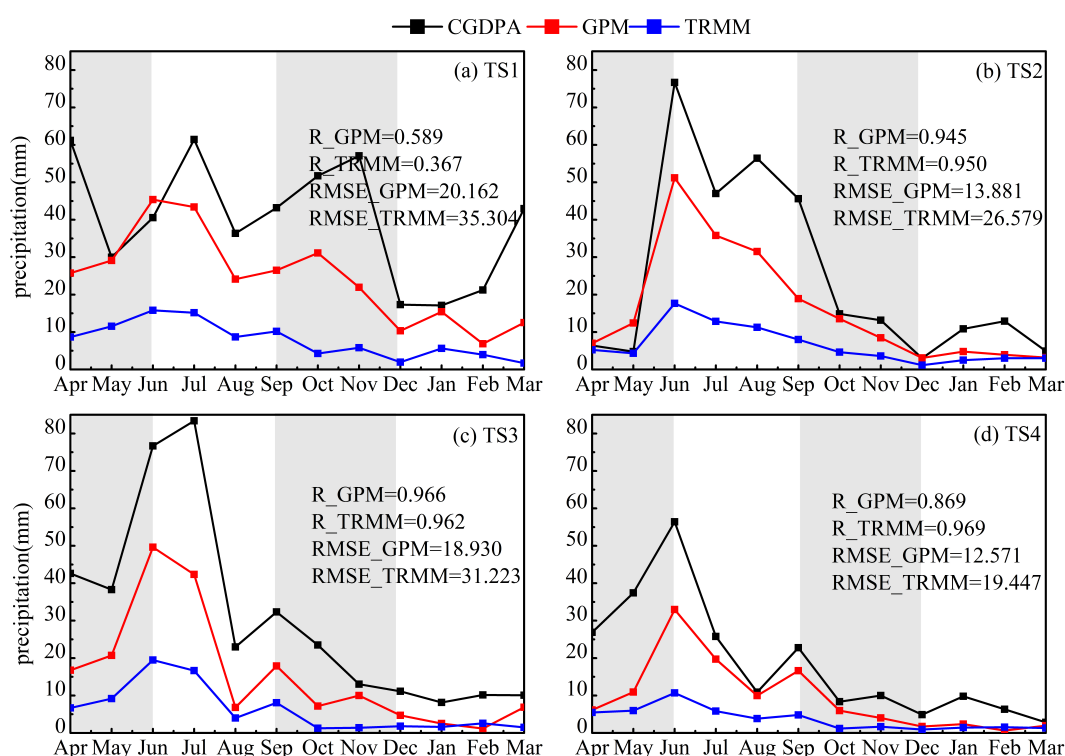

Figure 6. Annual variation in precipitation in four subregions of the Tianshan Mountains.

To show the statistical comparison of the seasonal variation of precipitation in the TSM and its subregions in 2014, we plotted a standardized Taylor diagram [38] and provide a summary of the corresponding degree between the estimated and observed precipitation by considering three statistics: standard deviation (SD), R and RMSE. The normalized Taylor diagram uses the SD and RMSE of

the reference value and variable value divided by the SD of the reference value, which eliminates physical-unit quantities. The result is shown in Figure 7. Among these, the radial coordinate represents the standard deviation, shown in black dashed lines, and the green semicircle represents the RMSE. Meanwhile, the angular coordinate represents R value, which is shown in blue dashed lines. In these figures, CGDPA represents the ground reference dataset (CGDPA is the reference point), and the other values were derived from the satellite precipitation datasets in different seasons. The closer the points of satellite precipitation are to the reference points, the better the product is.
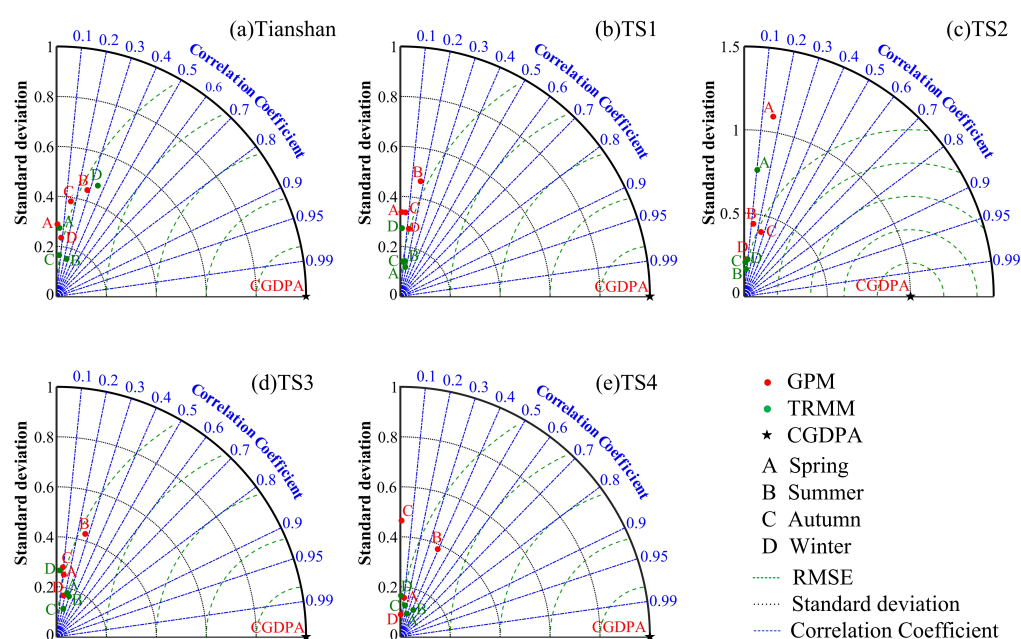

Figure 7. Taylor diagrams for the seasonal variation of precipitation in the TSM and the four subregions.

As shown in Figure 7, overall (Figure 7a), except for winter, the correlation between the two satellite datasets and the ground reference dataset shows the same trend as the seasonal variations, both of which show lower levels in spring and higher levels in summer and autumn. Among the four subregions (Figure 7b–e), TS2 shows significant seasonality, and the estimated summer spatial patterns of precipitation in TS3 and TS4 are better than the estimates for the other three seasons, with a lower RMSE and a higher correlation coefficient (R). All the products tend to underestimate the spatial variability of seasonal precipitation.

4.4. Probability Density Function

Figure 8 shows the performance of the PDF calculated based on the two satellite products (GPM/TRMM) and the ground reference dataset (CGDPA) in the TSM and its subregions. Overall, both of the satellites have great defects in the detection of heavy precipitation events, while they have relatively high accuracy for weak precipitation events. GPM underestimates the occurrence of both low rain rates (<2 mm/d) and high rain rates (>20 mm/d), and it overestimates the occurrence of middle rain rates (2–20 mm/d). In the middle rain rates (especially 2–5 mm/d), the occurrence of TRMM is significantly the highest when compared to the other products. All the datasets show that the highest percentage mostly occurs at the precipitation class of 2–5 mm/d, while the lowest percentage mostly occurs at the precipitation class of >10 mm/d. TRMM tends to find more precipitation events than the ground observations, and GPM has a similar tends compared to CGDPA at all the thresholds, which is closer to the measured data. Thus, the performance of GPM is better than that of TRMM at capturing all classes of rainfall events.
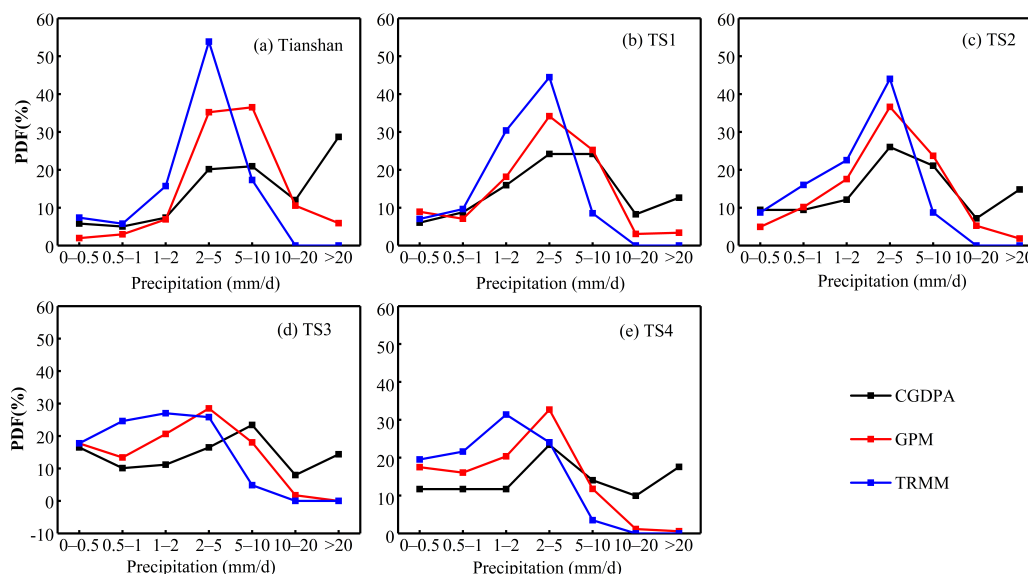
Figure 8. Probability density function (PDF) of precipitation estimation in Tianshan and four subregions.

4.5. Contingency Statistics

Finally, we examine rainy event detection using three statistics: POD, FAR and CSI. Table 3 lists the POD, FAR, FBI and CSI values of the GPM and TRMM datasets against CGDPA in the TSM and its subregions. Generally, both the GPM and TRMM have low PODs (<50%) and high FARs (>45%) over the different subregions, especially in northern China (such as Xinjiang) [39].

Table 3. Analysis of precipitation detection capability.

Name	POD		FAR		FBI		CSI	
	GPM	TRMM	GPM	TRMM	GPM	TRMM	GPM	TRMM
Tianshan	0.979	0.836	0.237	0.201	1.282	1.046	0.751	0.690
TS1	0.902	0.716	0.474	0.451	1.716	1.304	0.497	0.451
TS2	0.952	0.740	0.381	0.336	1.537	1.115	0.600	0.538
TS3	0.843	0.640	0.510	0.461	1.721	1.186	0.449	0.414
TS4	0.816	0.730	0.552	0.485	1.822	1.417	0.407	0.433

POD shows that GPM notably improves the precipitation detection over the TSM and the four subregions compared with the TRMM estimates. All three datasets show that the FAR is largest in east Tianshan and smallest in southwest Tianshan, but TRMM performs better for FBI. The CSI results show that TRMM is better than GPM in terms of rainfall detection in east Tianshan. The overall analyses show that the performances of GPM/TRMM rainfall estimates in northwest Tianshan (TS1) and southwest Tianshan (TS2) were better and achieved relatively higher PODs and CSIs and lower FARs than those in the other subregions.

Overall, except for slightly higher FAR and FBI values, the POD and CSI values of GPM have significantly improved compared to TRMM, especially the POD value. Therefore, for detecting the precipitation frequency, GPM is better than TRMM.

5. Discussion

Previous studies have shown that satellite precipitation products do not perform well in Xinjiang, China [40]. However, in this study, we evaluated the GPM/TRMM datasets on different temporal scales (annual, seasonal, and daily) and it was found that GPM showed significant improvement compared with its predecessor TRMM. From the above analyses, it can be seen that the GPM-IMERG and TRMM datasets show obvious spatial differences in the precipitation estimation of TSM, with greater

precipitation in the north than the south and in the west than the east (Figure 2). The seasonal pattern is that the precipitation is more in summer and less in winter. Both satellite products can track and observe the spatial variation of precipitation. This is consistent with other results [26]. The main reason for the formation of this feature is that the large-scale mountain of TSM intercepted and uplifted the water vapor from Atlantic and Arctic Ocean, resulting in obvious precipitation gradient. Both satellite products underestimated annual precipitation, which is reasonable and has been reported in other high mountains areas [41,42]. Because arid areas have less rainfall and low water vapor in the atmosphere, it is difficult to detect by satellite sensors.

Based on daily evaluations, it is found that compared to TMPA, GPM products have improved R, POD, and CSI values. Such improvements have also been found in other studies [18,19]. The enhancement of these indicators of GPM products might be related to the improvements in the spatiotemporal resolution [21]. The GPM products provide precipitation estimates of 30 min intervals, while TRMM products provide estimates of 3 h periods. Due to the lower temporal resolution of TRMM products, however, some precipitation events are often missed, resulting in the lower R value. In addition, the influence of altitude on precipitation estimation for the two satellite products still exists. The R value is lower in high-elevation areas and higher in low-elevation areas. The performance of GPM/TRMM in high-elevation areas is worse than in low-elevation areas.

To more comprehensively evaluate the satellite datasets, we divided TSM into four subregions according to the geographical location and climatic conditions (Figure 1) and compared the satellite datasets and ground reference dataset across different subregions. In TS1 and TS3, the R value between GPM and CGDPA is greater than that of TRMM data, while in TS2 and TS4, the R value of GPM and CGDPA is slightly smaller than that of TRMM. GPM had a lower RMSE in the four subregions and performed better (Figure 6). Regarding seasonal changes, the two satellite products had a higher correlation in summer and autumn, and a lower correlation in winter and spring. Among the four subregions, TS2 showed significant seasonality (Figure 7). The reason may be that the winter and spring seasons in the study area are affected by the Siberian air mass, the precipitation is low, the weather is dry and cold, and the mountain surface is covered with snow. It is difficult for satellite products to distinguish between snow and clouds. In summer and autumn, the correlation increases as the precipitation increases under the influence of westerly winds from the Atlantic.

In addition, it is worth noting that both products overestimate moderate rainfall but underestimate heavy rainfall. In different subregions, except for the middle rain rate, the low rain rate and high rain rate of GPM precipitation datasets in TS1, TS2 and TS3 are better than TRMM, and are closer to the measured values. The performance of GPM on TS4 is better than that of TRMM. On the whole, GPM products are significantly better than TRMM products in TSM, especially in low rain rate and middle rain rate. As shown in Table 4, Fang et al. also reported similar results [19]. One possible reason is that the GMI and DPR sensors carried by the newly launched GPM satellite are better at detecting low and solid rain events, while the sensors carried by its pioneer TRMM are less sensitive to this [18].

Overall, the terrain of Tianshan Mountains was complex, and the meteorological stations were sparse. The interpolation of rain gauge data leads to the uncertainty of precipitation estimation in TSM. Therefore, it is necessary to estimate the satellite precipitation for TSM research. The study area here is divided according to geographical location and climatic conditions, and its performance is evaluated and analyzed based on the daily GPM and TRMM datasets from 2014 to 2015. Despite the uncertainties, the findings are still very valuable. Compared with TRMM datasets, GPM has higher temporal and spatial resolution and larger coverage, which is of great significance to the future research and application of meteorology, hydrology and natural disasters. In our next work, the TSM will be divided according to the different surface types and topographic factors, and monthly datasets will be used to analyze, evaluate and calibrate the satellite datasets in the TSM for a long time series to obtain more accurate precipitation information.

Table 4. The performance of CGDPA, GPM and TRMM in TSM and its subregions.

	The Frequency of Precipitation (%)	CGDPA	GPM	TRMM
	low rain rate	18.22	11.84	28.85
Tianshan	middle rain rate	53.10	82.24	71.15
	high rain rate	28.68	5.92	0.00
	low rain rate	30.77	34.15	47.04
TS1	middle rain rate	56.59	62.46	52.96
	high rain rate	12.64	3.38	0.00
	low rain rate	30.94	32.62	47.27
TS2	middle rain rate	54.26	65.54	52.73
	high rain rate	14.80	1.85	0.00
	low rain rate	37.77	51.74	69.35
TS3	middle rain rate	47.87	48.26	30.65
	high rain rate	14.36	0.00	0.00
	low rain rate	35.09	53.87	72.47
TS4	middle rain rate	47.37	45.56	27.53
	high rain rate	17.54	0.57	0.00

6. Conclusions

Based on daily-scale data, this study evaluated the GPM/TRMM products over the TSM from 1 April 2014 to 31 March 2015, using the CGDPA dataset as the reference. Three main statistical indicators (CV, R and RB) were used to compare GPM with TRMM and verify their abilities for measuring annual, seasonal and daily precipitation. We also studied the PDF and the satellite products' precipitation detection abilities. The main findings are as follows:

1. In 2014, GPM/TRMM captured the spatial variability of annual precipitation detected in the TSM area well, showing high precipitation in the TS1 and low precipitation in the TS4. The seasonal precipitation distribution is similar to that of annual precipitation. Both GPM and TRMM underestimated the annual precipitation, but GPM had a lower RMSE than TRMM. According to the seasonal analysis, both products underestimate the spatial variability of seasonal precipitation. Middle Tianshan and east Tianshan have the best estimated summer precipitation, with lower RMSE and higher R.

2. On a daily scale, GPM and TRMM obviously underestimate the larger CV values. Overall, GPM performs better than TRMM in detecting precipitation events. GPM is superior to TRMM with regard to the POD and CSI, where the POD is significantly higher. As for the FAR and FBI, TRMM is slightly better than GPM. The detection capabilities of the GPM/TRMM for precipitation events in the middle and east of Tianshan are significantly lower than in the northwest and southwest.

3. The influence of terrain on precipitation: the study found that the influence of terrain on satellite precipitation estimation still exists. The R value is lower in high-elevation area and higher in low-elevation area, indicating that more improvement should be made in high-elevation areas.

4. By comparing the PDF, GPM shows a trend of underestimating low rain rate and high rain rate events but overestimating middle rain rate events, while TRMM tends to find more events than the ground observations. Compared with TRMM, GPM's PDF values on all thresholds are similar to the CGDPA trends; therefore, the GPM dataset performs better than TRMM at capturing all types of rainfall events.

5. Performance of GPM/TRMM in subregions: In TS1 and TS3, the correlation between GPM and CGDPA is greater than that of TRMM, while in TS2 and TS4, the R value of GPM is slightly less than that of TRMM. GPM has lower RMSE in all subregions and performs better.

The results of this study show that GPM exhibits significant improvements compared to its predecessor, TRMM 3B42V7. It can show more spatial details and has a better application prospect. Considering the performance of GPM in different subregions and the underestimation of high-elevation precipitation, the data need to be further corrected to better reflect the precipitation information of high-latitude and high-altitude area in arid areas so as to alleviate the difficulties of collecting ground observation data in complex terrain and scarce data area.

Author Contributions: Conceptualization, Y.Z., G.H., S.D. and Z.X.; methodology, Y.Z. and S.D.; writing—original draft preparation, Y.Z.; writing—review and editing, Y.Z., S.D. and Q.L. All authors have read and agreed to the published version of the manuscript.

Conflicts of Interest: The authors declare no conflict of interest.

References

1. Wang, X.; Ding, Y.; Zhao, C.; Wang, J. Similarities and improvements of GPM IMERG upon TRMM 3B42 precipitation product under complex topographic and climatic conditions over Hexi region, Northeastern Tibetan Plateau. *Atmos. Res.* **2019**, *218*, 347–363. [CrossRef]
2. Lu, D.; Yong, B. Evaluation and Hydrological Utility of the Latest GPM IMERG V5 and GSMaP V7 Precipitation Products over the Tibetan Plateau. *Remote Sens.* **2018**, *10*, 2022. [CrossRef]
3. Prakash, S.; Mitra, A.K.; Pai, D.S.; Aghakouchak, A. From TRMM to GPM: How well can heavy rainfall be detected from space? *Adv. Water Resour.* **2016**, *88*, 1–7. [CrossRef]
4. Zhang, A.; Xiao, L.; Min, C.; Chen, S.; Kulie, M.; Huang, C.; Liang, Z. Evaluation of latest GPM-Era high-resolution satellite precipitation products during the May 2017 Guangdong extreme rainfall event. *Atmos. Res.* **2019**, *216*, 76–85. [CrossRef]
5. Jiang, S.; Ren, L.; Xu, C.-Y.; Yong, B.; Yuan, F.; Liu, Y.; Yang, X.; Zeng, X. Statistical and hydrological evaluation of the latest Integrated Multi-satellitE Retrievals for GPM (IMERG) over a midlatitude humid basin in South China. *Atmos. Res.* **2018**, *214*, 418–429. [CrossRef]
6. Sun, Q.; Miao, C.; Duan, Q.; Ashouri, H.; Sorooshian, S.; Hsu, K.-L. A Review of Global Precipitation Data Sets: Data Sources, Estimation, and Intercomparisons. *Rev. Geophys.* **2018**, *56*, 79–107. [CrossRef]
7. Zhang, Q.; Shi, P.; Singh, V.P.; Fan, K.; Huang, J. Spatial downscaling of TRMM-based precipitation data using vegetative response in Xinjiang, China. *Int. J. Climatol.* **2017**, *37*, 3895–3909. [CrossRef]
8. Chen, S.; Hu, J.; Zhang, Z.; Behrangi, A.; Hong, Y.; Gebregiorgis, A.S.; Cao, J.; Hu, B.; Xue, X.; Zhang, X. Hydrologic Evaluation of the TRMM Multisatellite Precipitation Analysis Over Ganjiang Basin in Humid Southeastern China. *IEEE J. Sel. Top. Appl. Earth Obs. Remote Sens.* **2015**, *8*, 4568–4580. [CrossRef]
9. Hong, Y.; Adler, R.F.; Negri, A.; Huffman, G.J. Flood and landslide applications of near real-time satellite rainfall products. *Nat. Hazards* **2007**, *43*, 285–294. [CrossRef]
10. Huffman, G.J.; Adler, R.F.; Bolvin, D.T.; Gu, G.; Nelkin, E.J.; Bowman, K.P.; Hong, Y.; Stocker, E.F.; Wolff, D.B. The TRMM multisatellite precipitation analysis (TMPA): Quasi-global, multiyear, combined-sensor precipitation estimates at fine scales. *J. Hydrometeorol.* **2007**, *8*, 38–55. [CrossRef]
11. Li, X.-H.; Zhang, Q.; Xu, C.-Y. Suitability of the TRMM satellite rainfalls in driving a distributed hydrological model for water balance computations in Xinjiang catchment, Poyang lake basin. *J. Hydrol.* **2012**, *426*, 28–38. [CrossRef]
12. Su, F.; Hong, Y.; Lettenmaier, D.P. Evaluation of TRMM Multisatellite Precipitation Analysis (TMPA) and its utility in hydrologic prediction in the La Plata Basin. *J. Hydrometeorol.* **2008**, *9*, 622–640. [CrossRef]
13. Yang, N.; Zhang, K.; Hong, Y.; Zhao, Q.; Huang, Q.; Xu, Y.; Xue, X.; Chen, S. Evaluation of the TRMM multisatellite precipitation analysis and its applicability in supporting reservoir operation and water resources management in Hanjiang basin, China. *J. Hydrol.* **2017**, *549*, 313–325. [CrossRef]

14. Hou, A.Y.; Kakar, R.K.; Neeck, S.; Azarbarzin, A.A.; Kummerow, C.D.; Kojima, M.; Oki, R.; Nakamura, K.; Iguchi, T. The Global Precipitation Measurement Mission. *Bull. Am. Meteorol. Soc.* **2014**, *95*, 701–722. [CrossRef]

15. Liu, C.; Zipser, E.J. The global distribution of largest, deepest, and most intense precipitation systems. *Geophys. Res. Lett.* **2015**, *42*, 3591–3595. [CrossRef]

16. Wang, C.; Tang, G.; Han, Z.; Guo, X.; Hong, Y. Global intercomparison and regional evaluation of GPM IMERG Version-03, Version-04 and its latest Version-05 precipitation products: Similarity, difference and improvements. *J. Hydrol.* **2018**, *564*, 342–356. [CrossRef]

17. Mahmoud, M.T.; Hamouda, M.A.; Mohamed, M.M. Spatiotemporal evaluation of the GPM satellite precipitation products over the United Arab Emirates. *Atmos. Res.* **2019**, *219*, 200–212. [CrossRef]

18. Wu, Y.; Zhang, Z.; Huang, Y.; Jin, Q.; Chen, X.; Chang, J. Evaluation of the GPM IMERG v5 and TRMM 3B42 v7 Precipitation Products in the Yangtze River Basin, China. *Water* **2019**, *11*, 1459. [CrossRef]

19. Fang, J.; Yang, W.; Luan, Y.; Du, J.; Lin, A.; Zhao, L. Evaluation of the TRMM 3B42 and GPM IMERG products for extreme precipitation analysis over China. *Atmos. Res.* **2019**, *223*, 24–38. [CrossRef]

20. Tong, K.; Su, F.; Yang, D.; Hao, Z. Evaluation of satellite precipitation retrievals and their potential utilities in hydrologic modeling over the Tibetan Plateau. *J. Hydrol.* **2014**, *519*, 423–437. [CrossRef]

21. Caracciolo, D.; Francipane, A.; Viola, F.; Noto, L.V.; Deidda, R. Performances of GPM satellite precipitation over the two major Mediterranean islands. *Atmos. Res.* **2018**, *213*, 309–322. [CrossRef]

22. Li, Q.; Yang, T.; Zhang, F.; Qi, Z.; Li, L. Snow depth reconstruction over last century: Trend and distribution in the Tianshan Mountains, China. *Glob. Planet. Chang.* **2019**, *173*, 73–82. [CrossRef]

23. Ji, X.; Chen, Y. Characterizing spatial patterns of precipitation based on corrected TRMM B-3(43) data over the mid Tianshan Mountains of China. *J. Mt. Sci.* **2012**, *9*, 628–645. [CrossRef]

24. Mou Leong, T.; Santo, H. Comparison of GPM IMERG, TMPA 3B42 and PERSIANN-CDR satellite precipitation products over Malaysia. *Atmos. Res.* **2018**, *202*, 63–76. [CrossRef]

25. Lu, X.; Wei, M.; Tang, G.; Zhang, Y. Evaluation and correction of the TRMM 3B43V7 and GPM 3IMERGM satellite precipitation products by use of ground-based data over Xinjiang, China. *Environ. Earth Sci.* **2018**, *77*, 209. [CrossRef]

26. Fan, M.; Xu, J.; Chen, Y.; Li, W. Simulating the precipitation in the data-scarce Tianshan Mountains, Northwest China based on the Earth system data products. *Arab. J. Geoences* **2020**, *13*, 637. [CrossRef]

27. Zhao, C.; Yao, S.; Li, Q. The Distribution of Precipitation and Rain Days over the Tianshan Mountains in Northwest of China. *Earth Environ. Sci.* **2020**, *428*, 012063. [CrossRef]

28. Feng, G.; Yuhu, Z.; Qiuhua, C.; Peng, W.; Huirong, Y.; Yunjun, Y.; Wanyuan, C. Comparison of two long-term and high-resolution satellite precipitation datasets in Xinjiang, China. *Atmos. Res.* **2018**, *212*, 150–157.

29. Yang, M.; Li, Z.; Anjum, M.N.; Gao, Y. Performance Evaluation of Version 5 (V05) of Integrated Multi-Satellite Retrievals for Global Precipitation Measurement (IMERG) over the Tianshan Mountains of China. *Water* **2019**, *11*, 1139. [CrossRef]

30. Gao, L.; Wei, J.; Wang, L.; Bernhardt, M.; Schulz, K. A high-resolution air temperature data set for the Chinese Tian Shan in 1979–2016. *Earth Syst. Sci. Data* **2018**, *10*, 2097–2114. [CrossRef]

31. Guo, L.; Li, L. Variation of the proportion of precipitation occurring as snow in the Tian Shan Mountains, China. *Int. J. Climatol.* **2015**, *35*, 1379–1393. [CrossRef]

32. Prakash, S.; Mitra, A.K.; Aghakouchak, A.; Liu, Z.; Norouzi, H.; Pai, D.S. A preliminary assessment of GPM-based multi-satellite precipitation estimates over a monsoon dominated region. *J. Hydrol.* **2016**, *556*, 865–876. [CrossRef]

33. Peng, B.; Shi, J.; Ni-Meister, W.; Zhao, T.; Ji, D. Evaluation of TRMM Multisatellite Precipitation Analysis (TMPA) Products and Their Potential Hydrological Application at an Arid and Semiarid Basin in China. *IEEE J. Sel. Top. Appl. Earth Obs. Remote Sens.* **2014**, *7*, 3915–3930. [CrossRef]

34. Elhamid, A.M.I.A.; Eltahan, A.M.H.; Mohamed, L.M.E.; Hamouda, I.A. Assessment of the two satellite-based precipitation products TRMM and RFE rainfall records using ground based measurements. *AEJ Alex. Eng. J.* **2020**, *59*, 1049–1058. [CrossRef]

35. He, Z.; Yang, L.; Tian, F.; Ni, G.; Hou, A.; Lu, H. Intercomparisons of Rainfall Estimates from TRMM and GPM Multisatellite Products over the Upper Mekong River Basin. *J. Hydrometeorol.* **2017**, *18*, 413–430. [CrossRef]

36. Shen, Y.; Xiong, A. Validation and comparison of a new gauge-based precipitation analysis over mainland China. *Int. J. Climatol.* **2016**, *36*, 252–265. [CrossRef]

37. Yang, X.; Yong, B.; Hong, Y.; Chen, S.; Zhang, X. Error analysis of multi-satellite precipitation estimates with an independent raingauge observation network over a medium-sized humid basin. *Hydrol. Sci. J.* **2016**, *61*, 1813–1830. [CrossRef]

38. Taylor, K.E. Summarizing multiple aspects of model performance in a single diagram. *J. Geophys. Res. Atmos.* **2001**, *106*, 7183–7192. [CrossRef]

39. Guo, H.; Chen, S.; Bao, A.; Behrangi, A.; Hong, Y.; Ndayisaba, F.; Hu, J.; Stepanian, P.M. Early assessment of Integrated Multi-satellite Retrievals for Global Precipitation Measurement over China. *Atmos. Res.* **2016**, *176*, 121–133. [CrossRef]

40. Chen, F.; Li, X. Evaluation of IMERG and TRMM 3B43 Monthly Precipitation Products over Mainland China. *Remote Sens.* **2016**, *8*, 472. [CrossRef]

41. Ma, Z.; Xu, J.; Zhu, S.; Yang, J.; Hong, Y. AIMERG: A new Asian precipitation dataset (0.1°/half-hourly, 2000–2015) by calibrating the GPM-era IMERG at a daily scale using APHRODITE. *Earth Syst. Sci. Data* **2020**, *12*, 1525–1544. [CrossRef]

42. Sharma, S.; Chen, Y.; Zhou, X.; Yang, K.; Khadka, N. Evaluation of GPM-Era Satellite Precipitation Products on the Southern Slopes of the Central Himalayas Against Rain Gauge Data. *Remote Sens.* **2020**, *12*, 1836. [CrossRef]

Publisher's Note: MDPI stays neutral with regard to jurisdictional claims in published maps and institutional affiliations.